ORIGINAL STUDY

THERMODYNAMICS AND ELASTIC PROPERTIES OF TERNARY ALLOYS OF PD, PT, AND RH METALS: A MOLECULAR DYNAMICS SIMULATION STUDY

Yeshim Sarıbek[1], Zhangabay Turar[1], Arystanbek Kussainov[2], Rakhmetova Mairagul[3], Ali Coruh[1]

[1]Department of Physics, Sakarya University, Sakarya, Turkey
[2]Protectivie and Functional Coatings Scientific Center, Daulet Serikbayev East Kazakhstan Technical University Ust-Kamenogorsk 070010, Kazakhstan
[3]Department of Plasma Physics and Computer Physics, Al-Farabi Kazakh National University, Almaty, Kazakhstan/ Department of Physics and Technical disciplines, Kh. Dosmukhamedov Atyrau University, Atyrau, Kazakhstan;
*Corresponding author: coruh@sakarya.edu.tr

Abstract. *Thermodynamic and mechanical properties of multicomponent noble-metal alloys determine their performance in catalytic systems, energy-storage devices, and high-temperature structural materials. In the present work, temperature-dependent properties of four face-centered cubic ternary alloys of the Pd-Pt-Rh system with compositions $Pd_{15}Pt_{10}Rh_{75}$, $Pd_5Pt_{25}Rh_{70}$, $Pd_5Pt_{70}Rh_{25}$, and $Pd_{75}Pt_{15}Rh_{10}$ have been investigated by large-scale molecular dynamics simulations using the quantum Sutton-Chen potential. Calculations were performed for a supercell containing 1372 atoms in constant-enthalpy-constant-pressure, isothermal-isobaric, and microcanonical ensembles over a wide temperature range. It was found that the $Pd_5Pt_{70}Rh_{25}$ alloy exhibits the highest density, cohesive energy, and bulk modulus due to its high platinum content, which provides the strongest interatomic bonding. All studied compositions show negative enthalpy of formation, indicating thermodynamic stability; however, the $Pd_{75}Pt_{15}Rh_{10}$ alloy demonstrates the lowest miscibility. The heat capacity and thermal expansion coefficient calculated at 300 K are in good agreement with experimental data for pure palladium, platinum, and rhodium, confirming the validity of the chosen potential. Full sets of elastic constants and derived elastic moduli have been determined; all alloys satisfy mechanical stability criteria and exhibit ductile behavior, with $Pd_5Pt_{70}Rh_{25}$ being the most ductile. The results represent the first systematic molecular dynamics study of Pd-Pt-Rh ternary alloys and can be used for the design of next-generation catalytic and energy-related materials.*

Keywords: Molecular Dynamics, Quantum Sutton-Chen potential, ternary alloys, mechanical properties.

1. Introduction

Transition metals and their alloys constitute an essential class of materials underpinning numerous technological applications. Their remarkable mechanical strength, corrosion resistance, and catalytic performance make them indispensable in fields such as medicine, aerospace engineering, and micro-technologies. In particular, Pd, Pt, and Rh and their corresponding alloys are widely employed in automotive and space industries, medical devices, and dental applications. These metals have recently gained even greater prominence due to their critical role in automotive exhaust-gas catalysts, which are increasingly important as global efforts intensify to reduce CO_2 emissions and mitigate climate change [1]. Moreover, with the rapid expansion of hydrogen-based energy systems, Pd-, Pt-, and Rh-based materials have attracted substantial interest because of their exceptional hydrogen absorption and retention capacities [2]. The strategic importance of these elements has further stimulated advancements in recycling technologies, and the recovery of Pd, Pt, and Rh from spent automotive catalysts now represents a significant industrial sector [3,4].

Molecular dynamics (MD) simulations have played a central role in understanding metals and alloys at the atomic scale. MD allows for time-resolved analysis of thermodynamic, structural, and dynamical properties

Received 4 December 2025; revised 17 December 2025; accepted 5 January 2026.
Published online 20 March 2026

(https:doi.org/……)

[5,6], providing access to interatomic forces derived from the gradients of appropriately chosen potential functions [7]. Classical MD simulations typically employ empirical many-body potentials; however, early formulations were often insufficient to capture the complex characteristics of metallic bonding. To address this, refined potentials incorporating local electronic density or volume-dependent many-body interactions were developed, enabling significantly improved representations of metallic cohesion [7-14].

Among these, the Sutton-Chen (SC) potential has been widely utilized due to its simple power-law functional form, computational efficiency, and ability to reproduce experimental lattice parameters, cohesive energies, and bulk moduli of FCC metals [15]. Nevertheless, the original SC potential was subsequently reparametrized by Kimura, Cagın, and colleagues to incorporate temperature-dependent physical properties more accurately. By fitting additional observables-including phonon frequencies at the X-point-and accounting for zero-point energy (ZPE), they formulated the Quantum Sutton-Chen (Q-SC) potential [16]. This enhanced potential has since been applied extensively to studies of glass formation, crystallization, surface energetics, cluster and nanowire behavior, and single-crystal plasticity in FCC metals [17-19].

Several notable investigations have highlighted the effectiveness of the Q-SC model. Kart H.H. et al. examined Pd, Ag, and their alloys, revealing distinct differences between predictions obtained from SC and Q-SC potentials [20]. Kart S.O. and collaborators further explored Pd-Ni systems in solid, liquid, and amorphous phases using both potentials, demonstrating superior accuracy with Q-SC [21]. Davoodi and Moradi investigated temperature effects on the mechanical behavior of ordered Pd_3Rh and $PdRh_3$ alloys [22], while Ning and Hu analyzed the strengthening induced by Ru and Ce in Pt-Pd-Rh systems [23]. Luyten et al. studied phase behavior in Pd-Pt-Rh alloys using MEAM potentials, reporting exothermic alloy-formation reactions across a range of compositions [24]. In addition, Sakamoto et al. examined hydrogen absorption thermodynamics in Pd-Pt-Rh ternary alloys, emphasizing their potential in hydrogen-storage applications [25]. Despite these efforts, studies focusing simultaneously on the thermal and mechanical behavior of Pd-Pt-Rh ternary systems remain limited compared to their binary counterparts.

To fill this gap, the present work provides a comprehensive theoretical investigation of four ternary alloys-$Pd_{15}Pt_{10}Rh_{75}$, $Pd_5Pt_{25}Rh_{70}$, $Pd_5Pt_{70}Rh_{25}$, and $Pd_{75}Pt_{15}Rh_{10}$-over a broad temperature range. We report detailed predictions of lattice parameters, cohesive energies, densities, enthalpies, heat capacities, thermal expansion coefficients, and elastic constants, along with derived quantities such as bulk, shear, and Young's moduli, Poisson's ratios, and G/B ratios. Furthermore, we evaluate ductility, brittleness, elastic response, and hardness for these compositions for the first time, providing new insights into the structure-property relationships of Pd-Pt-Rh ternary alloys.

2. Method of calculation

The empirical many-body Finnis-Sinclair force field includes a repulsive and an attractive term, proportional to the square root of the local density. Total potential energy of metals and alloys per atom in a system of N atoms is given by:

$$U_{tot} = \sum_i U_i = \sum_i \left[\sum_{j \neq i} \epsilon_{ij} \frac{1}{2} V(r_{ij}) - c_i \epsilon_{ij} (\rho_i)^{1/2} \right]. \quad (1)$$

$V(r_{ij})$ is a pair wise repulsive term between the ith and jth atoms. Second term describes the many body cohesive term associated with atom i,

$$V(r_{ij}) = \left(\frac{a_{ij}}{r_{ij}} \right)^{n_{ij}}, \quad (2)$$

and

$$\rho_i = \sum_{i \neq j} \emptyset(r_{ij}), \quad (3)$$

$$\emptyset(r_{ij}) = \left(\frac{a_{ij}}{r_{ij}} \right)^{m_{ij}}. \quad (4)$$

Where r_{ij} is the distance between the ith and jth atoms. a_{ij} is the length scale parameter leading to dimensionless arguments for $V(r_{ij})$ and ρ_i. Other parameters (namely c_{ij}, ε_{ij}, n_{ij}, and m_{ij}) are obtained by fitting the 0K properties, such as the zero-pressure condition, the cohesive energy, and the bulk modulus of the FCC pure metals. c_{ij} is a dimensionless parameter scaling the attractive term, ε_{ij} is an energy parameter obtained from experiments, and n_{ij}, m_{ij} are positive integer parameters with n>m. These integer parameters define the range of the two components of the potential. The values of the Q-SC potential parameters for Pd, Pt, and Rh are given in Table 1.

Table 1. The Q-SC potential parameters for Pd, Pt, and Rh pure metals [18,20].

Metal	Model	n	m	ε (eV)	c	a (A°)
Pd	Q-SC	12	6	0.32864E-2	148.205	3.8813
Pt	Q-SC	11	7	0.97894E-2	71.336	3.9163
Rh	Q-SC	13	5	0.24612E-2	305.499	3.7984

In this study, MD simulations are made for a supercell consisting of a 7x7x7 conventional unit cell. The algorithms of MD simulation are based on the extended Hamiltonian formalism, presented in the studies of Andersen [26], Parinello-Rahman [27], Nosé [28], Hoover [29], and Cagın and Pettitt [30]. The system is considered to be a cubic box with 1372 atoms, which is sufficient for statistics of the equilibrium properties, such as pressure, temperature, energy, etc. The simulation starts with atoms arbitrarily distributed on an FCC lattice subject to the periodic boundary conditions in three dimensions. A 5th-order gear predictor-corrector algorithm is used to integrate the equations of motion with a time step of 2 fs. The Parrinello-Rahman piston mass parameter is chosen as W=400, and the Nosé-Hoover parameter is set to Q=100. The cutoff distance for the interactions between the atoms is taken to be two lattice parameters to realize maximum capacity and speed of the calculations. However, the temperature effects are taken into account by extending the range an additional distance of half a lattice parameter. Three ensembles, namely HPN (constant enthalpy and constant pressure), TPN (constant pressure and constant temperature), and EVN (constant energy and constant volume), respectively, are used in the simulation. First, the system is heated from 0.1 K to the target temperature with increments of 200 K in the HPN ensemble. At each temperature, 2000 time steps are performed to equilibrate the system. In order to get more accurate values of the melting temperature, the system is heated up with increments of 10K near the melting temperature. Afterwards, the volume, density, and energy of the system are obtained in the TPN ensemble. 20000 additional steps are carried out for TPN dynamics. Finally, 50000 additional steps are performed in EVN ensemble conditions to obtain the elastic constants of the materials. The resultant zero-strain average matrix $<h_0>$ is used to obtain the pressure-dependent properties of the system in the EVN dynamics.

3. Results and discussion

3.1 Lattice parameters, cohesive energy, enthalpy, and density

Lattice parameters, cohesive energy, density, and enthalpy are evaluated in the TPN dynamics. The results for $Pd_{15}Pt_{10}Rh_{75}$, $Pd_5Pt_{25}Rh_{70}$, $Pd_5Pt_{70}Rh_{25}$, and $Pd_{75}Pt_{15}Rh_{10}$ alloys are given in Table 2. Since, to our knowledge, there exist no experimental data for ternary Pd-Pt-Rh alloys, we present the calculated results without comparison.

Table 2. Lattice parameter (a), density (ρ), cohesive energy (E_c), and enthalpy (H) for $Pd_{15}Pt_{10}Rh_{75}$, $Pd_5Pt_{25}Rh_{70}$, $Pd_5Pt_{70}Rh_{25}$, and $Pd_{75}Pt_{15}Rh_{10}$ alloys calculated from TPN ensemble at different temperatures using Q-SC potential parameters.

Metals	T (K)	a (Å)	ρ (g/cm^3)	H (kJ/mol)	E_c (kJ/mol)
$Pd_{15}Pt_{10}Rh_{75}$	0	3.813	13.49	-533.49	-533.28
	200	3.823	13.38	-528.24	-530.73
	400	3.834	13.27	-523.07	-528.06
	600	3.845	13.15	-517.84	-525.33
	800	3.856	13.04	-512.54	-522.52
	1000	3.868	12.91	-507.12	-519.60
$Pd_5Pt_{25}Rh_{70}$	0	3.826	14.95	-552.42	-552.18
	200	3.835	14.84	-547.22	-549.72
	400	3.845	14.73	-542.06	-547.05
	600	3.856	14.60	-536.84	-544.33
	800	3.867	14.48	-531.55	-541.54
	1000	3.878	14.35	-526.16	-538.63
$Pd_5Pt_{70}Rh_{25}$	0	3.879	19.05	-555.93	-555.68
	200	3.889	18.92	-550.78	-553.27

Table 2. (continued)

	400	3.899	18.77	-545.64	-550.63
	600	3.910	18.61	-540.44	-547.93
	800	3.921	18.45	-535.16	-545.14
	1000	3.933	18.29	-529.76	-542.24
$Pd_{75}Pt_{15}Rh_{10}$	0	3.868	13.69	-425.49	-425.32
	200	3.880	13.56	-420.31	-422.81
	400	3.893	13.42	-415.15	-420.15
	600	3.908	13.28	-409.90	-417.38
	800	3.923	13.13	-404.50	-414.49
	1000	3.939	12.97	-398.94	-411.42

In Fig. 1, one can notice that $Pd_5Pt_{70}Rh_{25}$ has the highest density depending on Pt concentration. Lattice parameters of $Pd_{75}Pt_{15}Rh_{10}$ and $Pd_5Pt_{70}Rh_{25}$ have nearly the same value at about 600 K, but the lattice parameter of $Pd_{75}Pt_{15}Rh_{10}$ slightly increases compared to $Pd_5Pt_{70}Rh_{25}$ alloy, depending on temperature. In Fig. 3, the enthalpy curve of $Pd_{75}Pt_{15}Rh_{10}$ has the highest values, which are in agreement with the information given in Fig. 2.

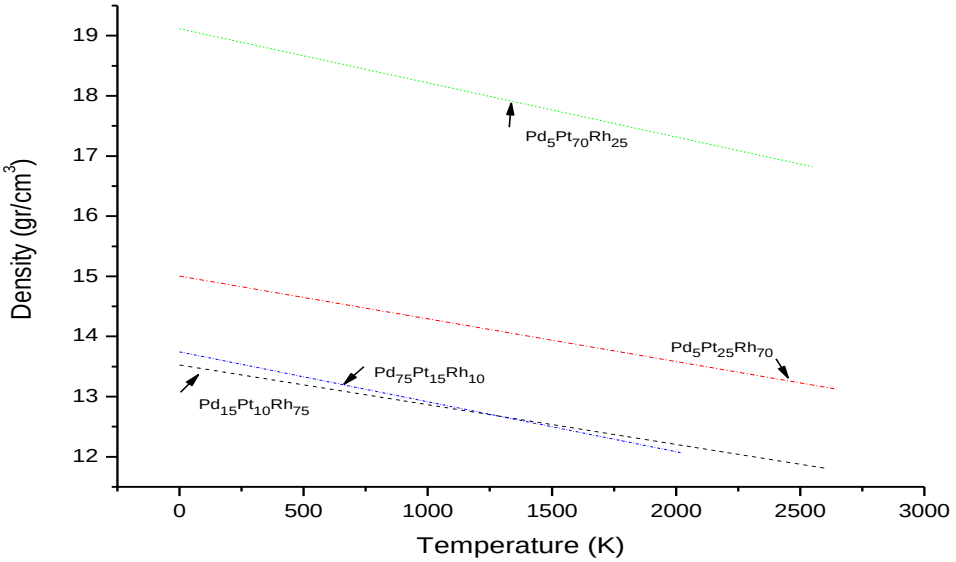

Fig. 1. Density of $Pd_{15}Pt_{10}Rh_{75}$, $Pd_5Pt_{25}Rh_{70}$, $Pd_5Pt_{70}Rh_{25}$ and $Pd_{75}Pt_{15}Rh_{10}$ alloys as a function of temperature for Q-SC potential parameters.

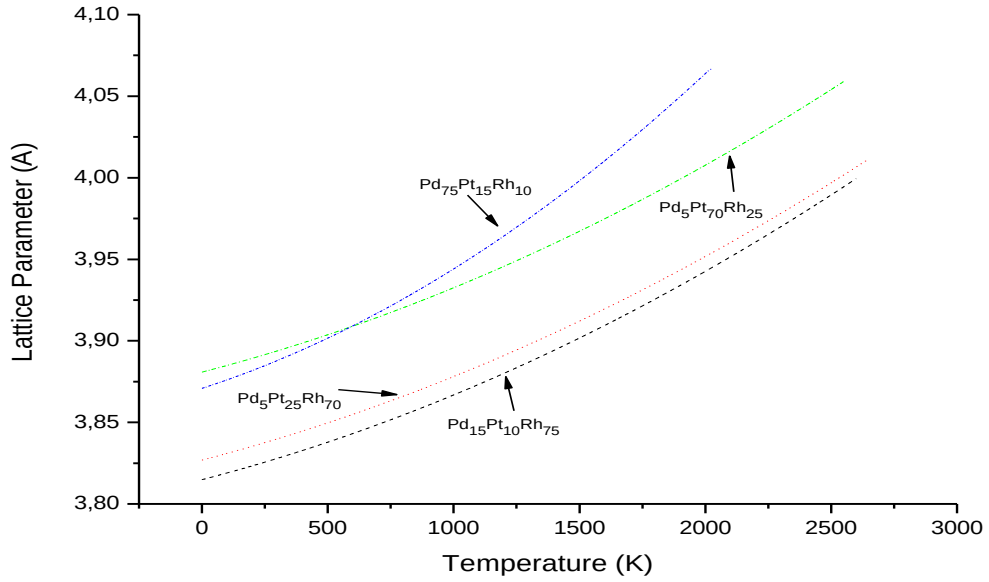

Fig. 2. Lattice parameters of $Pd_{15}Pt_{10}Rh_{75}$, $Pd_5Pt_{25}Rh_{70}$, $Pd_5Pt_{70}Rh_{25}$, and $Pd_{75}Pt_{15}Rh_{10}$ alloys as a function of temperature for Q-SC potential parameters.

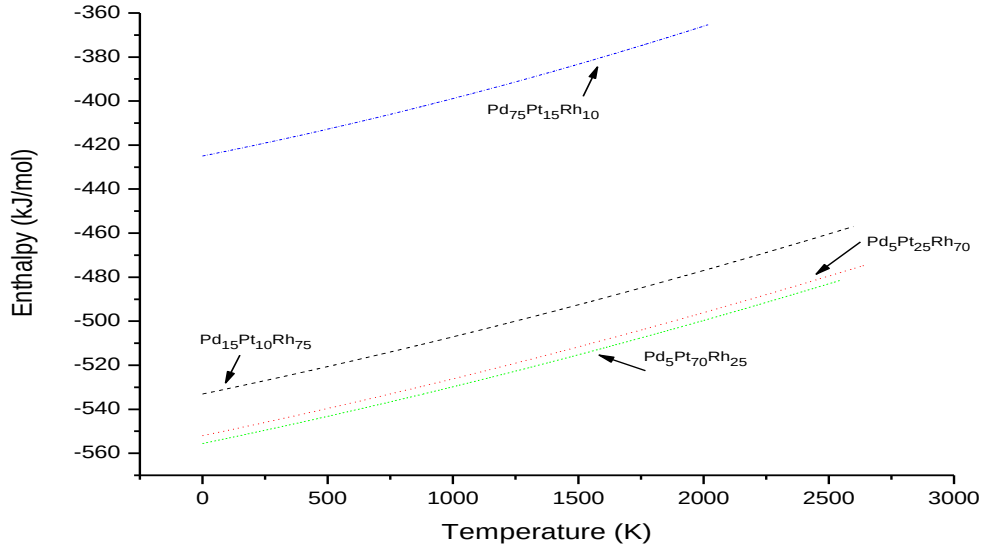

Fig. 3. Enthalpy of $Pd_{15}Pt_{10}Rh_{75}$, $Pd_5Pt_{25}Rh_{70}$, $Pd_5Pt_{70}Rh_{25}$, and $Pd_{75}Pt_{15}Rh_{10}$ alloys as a function of temperature for Q-SC potential parameters.

3.2 Specific heat capacity and thermal expansion coefficient

The calculated enthalpy results are fitted to a quadratic polynomial using the data below the melting temperature in order to investigate the specific heat capacity as a function of temperature. Fitted data lie between 200 and 2600 K for $Pd_{15}Pt_{10}Rh_{75}$, 200 and 2650 K for $Pd_5Pt_{25}Rh_{70}$, 200 and 2500 K for $Pd_5Pt_{70}Rh_{25}$, and 200 and 2020 K for $Pd_{75}Pt_{15}Rh_{10}$. The quadratic polynomial may be chosen as follows:

$$H(T) = a + bT + cT^2 \ \ (kJ\ mol^{-1}). \quad (5)$$

Where, T is the temperature. Specific heat capacity can be calculated by taking the first derivative of equation (5) as follows.

$$C_p(T) = \left(\frac{\partial H(T)}{\partial T}\right)_p. \quad (6)$$

We obtain a, b, and c from the fitted results of enthalpy data calculated from Q-SC potential parameters at each temperature. The coefficients of thermal expansion (a, b, and c) in Eq. (5), calculated by using the Q-SC potentials, are given in Table 3.

Table 3. Specific heat capacity calculated from Q-SC potential parameters for $Pd_{15}Pt_{10}Rh_{75}$, $Pd_5Pt_{25}Rh_{70}$, $Pd_5Pt_{70}Rh_{25}$, and $Pd_{75}Pt_{15}Rh_{10}$ alloys, and coefficients of the polynomial function used to find the heat capacity of alloys.

					C_p (kJ mole $^{-1}$ K^{-1})
Metals	a	b x 10^{-4}	c x 10^{-6}	Potential Model	Present Work
$Pd_{15}Pt_{10}Rh_{75}$	-533.079	239.200	2.064	Q-SC	0.0251584
$Pd_5Pt_{25}Rh_{70}$	-552.029	237.700	2.094	Q-SC	0.0250264
$Pd_5Pt_{70}Rh_{25}$	-555.560	236.300	2.156	Q-SC	0.0249236
$Pd_{75}Pt_{15}Rh_{10}$	-424.955	227.200	3.383	Q-SC	0.0247498

Experimental heat capacities of Pd, Pt, and Rh metals are 0.02598 kJ/mol K, 0.02586 kJ/mol K, and 0.02498 kJ/mol K, respectively [31]. It can be concluded from Table 3 that the simulated results for alloys and the experimental data given for metals are in good agreement at 300 K.

In order to examine the thermal expansion behavior, we have fitted the lattice parameter data below the melting temperature as a function of temperature to a quadratic polynomial similar to the heat capacity calculation:

$$a(T) = a + bT + cT^2 . \quad (7)$$

Thermal expansion coefficient is obtained by replacing the first derivative of Eq. (7) into Eq. (8),

$$\alpha_p(T) = -\frac{1}{a(T)}\left(\frac{\partial a(T)}{\partial T}\right)_p . \quad (8)$$

Table 4 includes the coefficients of Eq. (7), and the simulated results for thermal expansion coefficients (α) at 300 K. Experimental thermal expansion values of Pd, Pt and Rh metals are 1.18x10^{-5} K^{-1}, 0.88x10^{-5} K^{-1} and 0.82x10^{-5} K^{-1}, respectively [31], From Table 4, one can see that the simulated results for alloys and the experimental data given for metals are in good agreement.

Table 4. Thermal expansion coefficient calculated from Q-SC potential parameters for $Pd_{15}Pt_{10}Rh_{75}$, $Pd_5Pt_{25}Rh_{70}$, $Pd_5Pt_{70}Rh_{25}$, and $Pd_{75}Pt_{15}Rh_{10}$ alloys, and coefficients of the polynomial function used to find the thermal expansion coefficient of alloys.

					α_p x 10^{-5} (K^{-1})
Metals	a	b x 10^{-5}	c x10^{-8}	Potential Model	Present Work
$Pd_{15}Pt_{10}Rh_{75}$	3.81	4.00	1.19	Q-SC	1.2362
$Pd_5Pt_{25}Rh_{70}$	3.83	4.00	1.12	Q-SC	1.2208
$Pd_5Pt_{70}Rh_{25}$	3.88	4.00	1.17	Q-SC	1.2119
$Pd_{75}Pt_{15}Rh_{10}$	3.87	5.00	2.32	Q-SC	1.6520

3.3 Elastic constants, bulk modulus, shear modulus, and Young's modulus

The elastic constants of a solid provide information on the stability and stiffness of the material. We calculated the elastic constants by using the following fluctuation expression [32]:

$$C_{\alpha\beta\gamma\kappa} = \frac{\Omega_0}{k_B T}\left(\langle P_{\alpha\beta}P_{\gamma\kappa}\rangle - \langle P_{\alpha\beta}\rangle\langle P_{\gamma\kappa}\rangle\right) + \frac{2Nk_BT}{\Omega_0}\left(\delta_{\alpha\delta}\delta_{\beta\kappa} + \delta_{\alpha\kappa}\delta_{\beta\gamma}\right) + \langle\chi_{\alpha\beta\gamma\kappa}\rangle. \quad (9)$$

Here, the angular brackets symbolize averaging over time, and Ω_0=deth_0 is the reference volume for the model system. The first term indicates the contribution from the fluctuation of the microscopic stress tensor P_{ij}. The second term is the temperature correction term, which represents the kinetic energy contribution, and the last term denotes the contribution of the Born term to the elastic constants. Elastic constants are calculated by imposing an external strain on the crystal, relaxing any internal parameters to obtain the energy as a function

of the strain, and numerically solving for the elastic constants as the curvature of the energy versus strain curve [32]. The largest contribution to the elastic constants comes from the Born term in Eq. (9).

In this work, we have calculated the elastic constants from EVN simulations of 50000 steps for each alloy below the corresponding melting point. Bulk modulus (B), shear modulus (G_v, G_R, and G), G/B ratio, Cauchy pressure (C_{12}-C_{44}), Cauchy's ratio (C_{12}/C_{44}), Poisson ratio (ν), and Young's modulus (Y) have been calculated by using C_{11}, C_{12}, and C_{44} elastic constants.

The bulk modulus can be determined from:

$$B = \frac{(C_{11}+2C_{12})}{3} \quad (10)$$

In addition, shear modulus, G_v, G_R and G are calculated from the Voigt-Reuss-Hill arithmetic approximation based on the Voigt and Reuss bounds [33]:

$$G_V = \frac{C_{11}-C_{12}+3C_{44}}{5} \quad (11)$$

$$G_R = \frac{5(C_{11}-C_{12})C_{44}}{4C_{44}+3(C_{11}-C_{12})}. \quad (12)$$

The arithmetic average of Voigt and Reuss bounds is called as Voigt-Reuss-Hill approximations. The Voigt-Reuss-Hill arithmetic approximation based on the Voigt and Reuss bounds have been used for G, ν and Y [34]:

$$G = \frac{G_V+G_R}{2}. \quad (13)$$

Poisson's ratio [35] can be determined from:

$$\nu = \frac{C_{12}}{C_{11}+C_{12}}. \quad (14)$$

From the calculated values of the bulk modulus and Poisson's ratio, we have also estimated the Young modulus:

$$Y = 3B(1-2\nu). \quad (15)$$

Results are listed in Tables 5, 6, 7, and 8 for all the alloys studied.

To our knowledge, no experimental data exist for the calculated properties in Tables 5, 6, 7, and 8 for $Pd_{15}Pt_{10}Rh_{75}$, $Pd_5Pt_{25}Rh_{70}$, $Pd_5Pt_{70}Rh_{25}$, and $Pd_{75}Pt_{15}Rh_{10}$ alloys. Therefore, our simulated results are given without comparison.

Table 5. Elastic constants C_{11}, C_{12}, and C_{44} (in GPa) calculated from Q-SC potential parameters and Bulk modulus (in GPa), (C_{12}/C_{44}) Cauchy's ratio, Cauchy pressure (C_{12}-C_{44}) (in GPa), G_v, G_R and G shear modulus (in GPa) based on using Voigt-Reuss-Hill arithmetic approximation, (ν) Poisson's ratio and (Y) Young modulus (in GPa) calculated by using elastic constants for $Pd_{15}Pt_{10}Rh_{75}$ alloy.

Alloys	$Pd_{15}Pt_{10}Rh_{75}$					
T(K)	C_{11}(GPa)	C_{12}(GPa)	C_{44}(GPa)	B(GPa)	C_{12}-C_{44}	C_{12}/C_{44}
0	262.009	183.327	118.781	209.554	64.545	1.543
200	296.911	197.603	130.472	230.705	67.131	1.515
400	285.347	192.37	123.469	223.362	68.901	1.558
600	274.278	186.234	116.93	215.582	69.304	1.593
800	263.22	180.022	109.507	207.754	70.515	1.644
1000	251.783	174.780	102.934	200.448	71.847	1.698

T(K)	G_v	G_R	G	G/B	ν	Y
0	87.005	65.708	76.357	0.364	0.4117	111.073
200	98.145	79.024	88.584	0.384	0.3996	138.991
400	92.677	74.273	83.475	0.374	0.4027	130.417
600	87.767	70.335	79.051	0.367	0.4044	123.649
800	82.344	66.248	74.296	0.358	0.4061	116.989
1000	77.161	61.659	69.410	0.346	0.4097	108.554

Table 6. Elastic constants C_{11}, C_{12}, and C_{44} (in GPa) calculated from Q-SC potential parameters and Bulk modulus (in GPa), (C_{12}/C_{44}) Cauchy's ratio, Cauchy pressure (C_{12}-C_{44}) (in GPa), G_v, G_R, and G shear modulus (in GPa) based on Voigt-Reuss-Hill arithmetic approximation, (ν) Poisson's ratio, and (Y) Young modulus (in GPa) calculated by using elastic constants for $Pd_5Pt_{25}Rh_{70}$ alloy.

Alloys	$Pd_5Pt_{25}Rh_{70}$					
T(K)	C_{11}(GPa)	C_{12}(GPa)	C_{44}(GPa)	B(GPa)	C_{12}-C_{44}	C_{12}/C_{44}
0	265.709	189.235	115.728	214.726	73.507	1.635

Table 6. (continued)

Alloys	$Pd_5Pt_{25}Rh_{70}$					
T(K)	C_{11}(GPa)	C_{12}(GPa)	C_{44}(GPa)	B(GPa)	C_{12}-C_{44}	C_{12}/C_{44}
200	307.852	207.829	131.716	241.170	76.114	1.578
400	297.161	202.092	125.242	233.781	76.850	1.614
600	285.585	196.206	118.029	225.999	78.177	1.662
800	273.969	190.150	111.249	218.089	78.900	1.709
1000	262.986	183.856	104.007	210.233	79.849	1.768

T(K)	G_v	G_R	G	G/B	ν	Y
0	84.731	63.916	74.324	0.346	0.4160	108.284
200	99.034	79.659	89.347	0.370	0.4030	140.333
400	94.159	75.725	84.942	0.363	0.4048	133.552
600	88.693	71.255	79.974	0.354	0.4072	125.778
800	83.513	66.945	75.229	0.345	0.4097	118.160
1000	78.230	62.977	70.604	0.336	0.4115	111.688

Table 7. Elastic constants C_{11}, C_{12}, and C_{44} (in GPa) calculated from Q-SC potential parameters and Bulk modulus (in GPa), (C_{12}/C_{44}) Cauchy's ratio, Cauchy pressure (C_{12}-C_{44}) (in GPa), G_v, G_R, and G shear modulus (in GPa) based on Voigt-Reuss-Hill arithmetic approximation, (ν) Poisson's ratio, and (Y) Young modulus (in GPa) calculated by using elastic constants for $Pd_5Pt_{70}Rh_{25}$ alloy.

Alloys	$Pd_5Pt_{70}Rh_{25}$					
T(K)	C_{11}(GPa)	C_{12}(GPa)	C_{44}(GPa)	B(GPa)	C_{12}-C_{44}	C_{12}/C_{44}
0	276.975	204.986	103.884	228.982	101.102	1.973
200	301.515	213.337	116.799	242.730	96.538	1.827
400	290.902	206.82	110.93	234.847	95.89	1.864
600	273.661	194.736	104.091	221.045	90.645	1.871
800	255.470	182.23	98.076	206.643	84.154	1.858
1000	240.423	172.455	91.726	195.111	80.729	1.880

T(K)	G_v	G_R	G	G/B	ν	Y
0	76.728	59.212	67.970	0.297	0.4253	102.607
200	87.715	70.375	79.045	0.326	0.4144	124.716
400	83.374	67.009	75.192	0.320	0.4155	119.021
600	78.240	62.891	70.566	0.319	0.4157	111.738
800	73.494	58.683	66.088	0.320	0.4163	103.732
1000	68.629	54.611	61.620	0.316	0.4177	96.358

Table 8. Elastic constants C_{11}, C_{12}, and C_{44} (in GPa) calculated from Q-SC potential parameters and Bulk modulus (in GPa), (C_{12}/C_{44}) Cauchy's ratio, Cauchy pressure (C_{12}-C_{44}) (in GPa), G_v, G_R, and G shear modulus (in GPa) based on Voigt-Reuss-Hill arithmetic approximation, (ν) Poisson's ratio, and (Y) Young modulus (in GPa) calculated by using elastic constants for $Pd_{75}Pt_{15}Rh_{10}$ alloy.

Alloys	$Pd_{75}Pt_{15}Rh_{10}$					
T(K)	C_{11}(GPa)	C_{12}(GPa)	C_{44}(GPa)	B(GPa)	C_{12}-C_{44}	C_{12}/C_{44}
0	215.041	152.953	87.581	173.649	65.372	1.746
200	231.425	159.166	94.968	183.252	64.198	1.676
400	216.725	149.594	88.115	171.971	61.479	1.698
600	199.845	137.633	81.724	158.370	55.909	1.684
800	185.034	128.664	74.491	147.454	54.173	1.727
1000	172.576	120.964	69.671	138.168	51.293	1.736

T(K)	G_v	G_R	G	G/B	ν	Y
0	64.966	50.669	57.818	0.333	0.4156	102.607
200	71.433	57.507	64.470	0.352	0.4075	124.716
400	66.295	53.401	59.848	0.348	0.4084	119.021
600	61.477	49.502	55.489	0.350	0.4078	111.738
800	55.969	44.951	50.460	0.342	0.4102	103.732
1000	52.125	41.473	46.799	0.333	0.4121	96.358

Elastic constant and bulk modulus curves calculated from the Q-SC potential are given in Fig. 4, 5, 6, and 7. When we examine Fig. 4, 5, and 6, we identify that the elastic constants of $Pd_{75}Pt_{15}Rh_{10}$ are much weaker compared to those of other alloys.

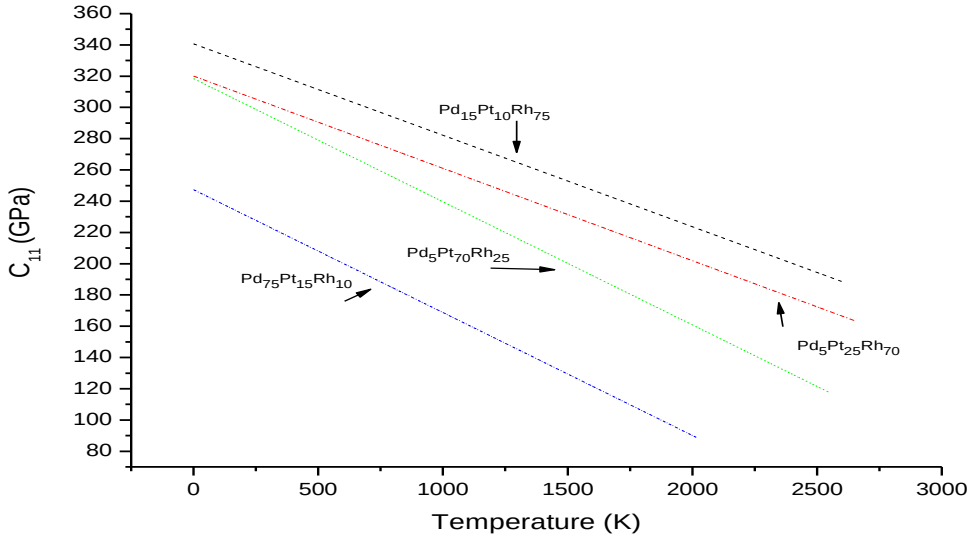

Fig. 4. Elastic constants C_{11} of $Pd_{15}Pt_{10}Rh_{75}$, $Pd_5Pt_{25}Rh_{70}$, $Pd_5Pt_{70}Rh_{25}$ and $Pd_{75}Pt_{15}Rh_{10}$ alloys as a function of temperature for Q-SC potential parameters.

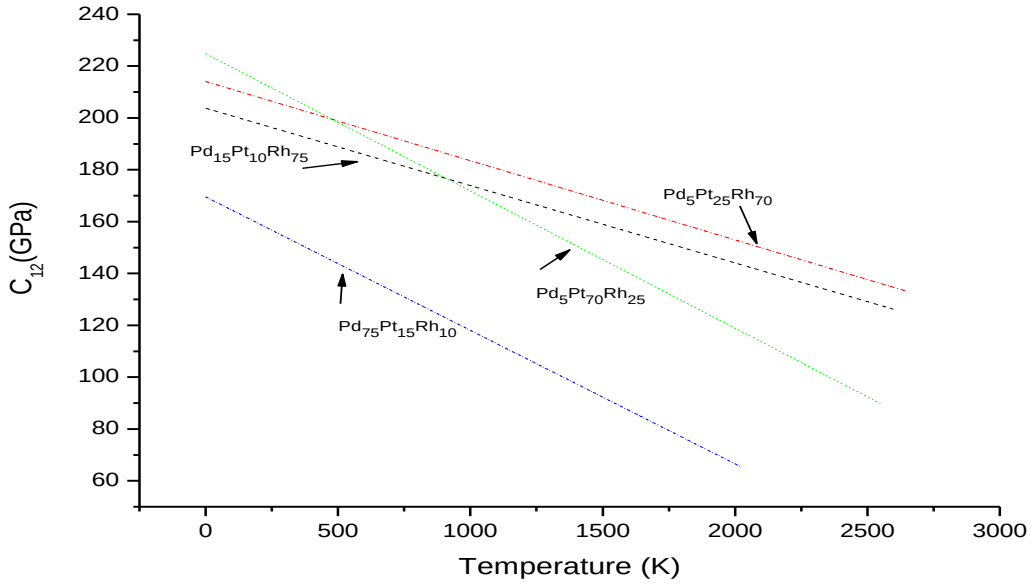

Fig. 5. Elastic constants C_{12} of $Pd_{15}Pt_{10}Rh_{75}$, $Pd_5Pt_{25}Rh_{70}$, $Pd_5Pt_{70}Rh_{25}$, and $Pd_{75}Pt_{15}Rh_{10}$ alloys as a function of temperature for Q-SC potential parameters.

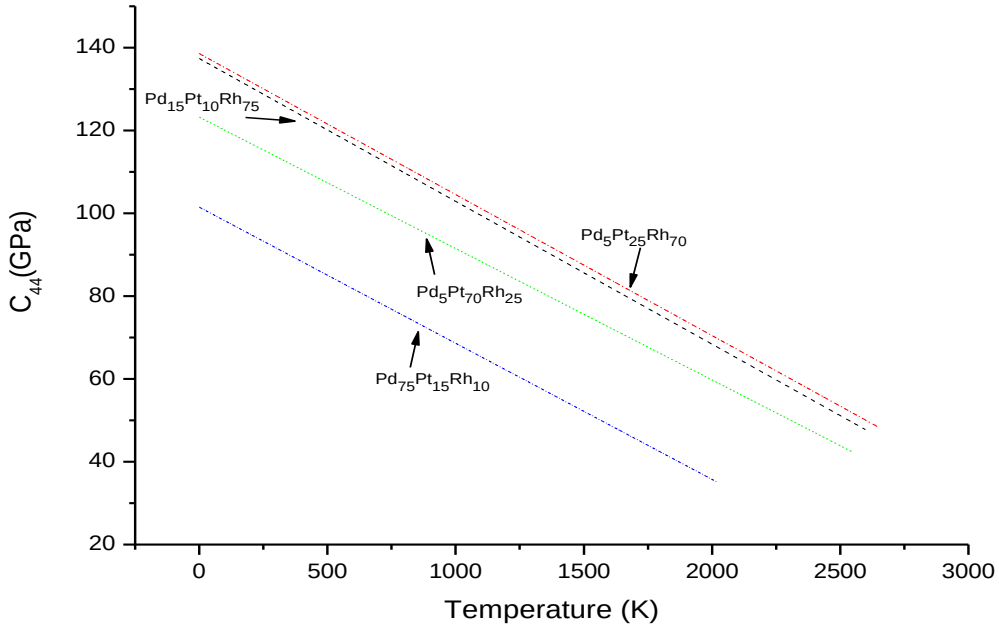

Fig. 6. Elastic constants C_{44} of $Pd_{15}Pt_{10}Rh_{75}$, $Pd_5Pt_{25}Rh_{70}$, $Pd_5Pt_{70}Rh_{25}$ and $Pd_{75}Pt_{15}Rh_{10}$ alloys as a function of temperature for Q-SC potential parameters.

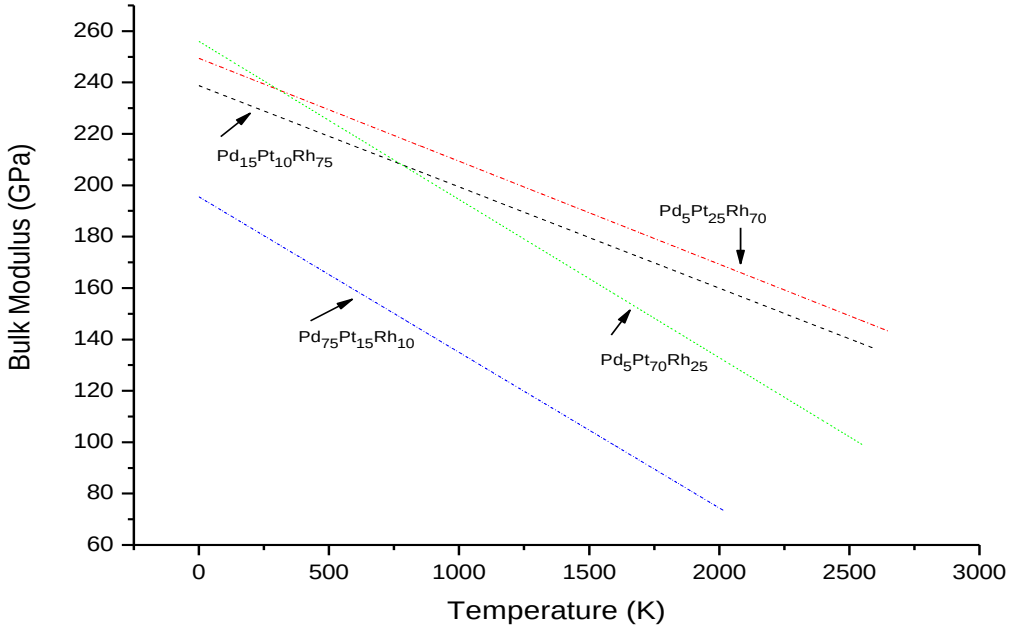

Fig. 7. Bulk modulus B of $Pd_{15}Pt_{10}Rh_{75}$, $Pd_5Pt_{25}Rh_{70}$, $Pd_5Pt_{70}Rh_{25}$, and $Pd_{75}Pt_{15}Rh_{10}$ alloys as a function of temperature for Q-SC potential parameters.

The average atomic bond strengths of $Pd_{15}Pt_{10}Rh_{75}$, $Pd_5Pt_{25}Rh_{70}$, $Pd_5Pt_{70}Rh_{25}$, and $Pd_{75}Pt_{15}Rh_{10}$ alloys based on the calculated bulk modulus (B) by using the Q-SC potential parameters follow the order from largest to smallest as $Pd_5Pt_{70}Rh_{25}$ > $Pd_5Pt_{25}Rh_{70}$ > $Pd_{15}Pt_{10}Rh_{75}$ > $Pd_{75}Pt_{15}Rh_{10}$. The experimental bulk modulus of Pd, Pt, and Rh metals is 181GPa, 278GPa, and 270 GPa [35,36], respectively. It seems that Pt has the highest average atomic bond strength. Thus, the average atomic bond strength of $Pd_5Pt_{70}Rh_{25}$ is larger compared to that of the other alloys, depending on Pt concentration.

The shear modulus (G) is related to the resistance of plastic deformation, while the bulk modulus (B) shows resistance to bond rupture. Therefore, it was reported that the ductile/brittle behavior of materials could be related empirically to their elastic constants by the ratio of G/B or Poisson's ratio. If G/B >0.5 or ν<1/3, the

material is brittle. Otherwise, the material is ductile [37, 38]. It can be concluded from the present study that G/B is smaller than 0.,5 and Poisson's ratio is larger than 1/3 for the alloys studied. It can be seen from the ratio G/B or Poisson's ratio (ν) that all alloys behave in a ductile manner.

Pettifor has suggested that the Cauchy pressure, which reflects the ductile/brittle behaviors of materials, could be used to describe the angular character of atomic bonding in metals and compounds. The Cauchy pressure is positive for metallic bonding, while it is negative for directional bonding. The ductile materials show positive Cauchy pressure; otherwise, the material is brittle [39]. If one looks at the Cauchy pressure of the alloys studied in the present work, it can be seen that all of them are positive. So, all of our simulated alloys are ductile in nature.

4. Conclusion

In this work, we have presented a wide range of properties of $Pd_{15}Pt_{10}Rh_{75}$, $Pd_5Pt_{25}Rh_{70}$, $Pd_5Pt_{70}Rh_{25,}$ and $Pd_{75}Pt_{15}Rh_{10}$ alloys. We have tried to understand the agreement of our results with experimental values of their metallic components.

It is seen in Fig. 6 that all of the enthalpy plots of studied alloys are in the negative region. It means that all of the alloys have exothermic behavior. It indicates that all the studied alloys are miscible, although $Pd_{75}Pt_{15}Rh_{10}$ has the least miscibility compared to the others. This information explains why the lattice parameters curve of $Pd_{75}Pt_{15}Rh_{10}$ sharply increases compared to those of other alloys (see Fig. 2).

In this study, we have calculated the bulk modulus (B), Cauchy pressure (C_{12}-C_{44}), Cauchy's ratio (C_{12}/C_{44}), shear modulus (G_v, $G_{R,}$ and G), G/B ratio, Poisson's ratio (ν), and Young's modulus (Y) by using C_{11}, $C_{12,}$ and C_{44} elastic constants results. Examining these results, we can say that all of the studied alloys are ductile. Depending on the G/B ratio, we can order the ductility of alloys as $Pd_5Pt_{70}Rh_{25}$ > $Pd_{15}Pt_{10}Rh_{75}$ > $Pd_5Pt_{25}Rh_{70}$> $Pd_{75}Pt_{15}Rh_{10}$.

During the study, we could not identify an eutectic alloy concentration that is possible between noble metal alloys. In our guess, Rh is the compound that prevents the alloys to be formed in eutectic form.

Funding

This work does not receive any funding.

Conflict of interest

The authors declare no conflict of interest.

Acknowledgements

This study is supported by SAÜ BAP 2007-02-02-004 Project of Sakarya University-TURKEY.

References

1 Davis, S., Salisbury, T., Pinson, G., Christianson, R., Berlin, M., Downey, J., Gleason, W., James, R., Rosenberg, E., Gleason, K., Hiebert, R., Mccloskey, J. (2012). Improved Palladium Coatings for Hydrogen Purification Membranes. *Energy Technology 2012: Carbon Dioxide Management and Other Technologies.* ch39, 323-330. DOI: 10.1002/9781118365038

2 James, R., Brenner., Gaurav, B., Pareen, V. (2008). Hydrogen purification with palladium and palladium alloys on porous stainless steel membranes. *Int. J. Oil, Gas and Coal Technology.* 1, 1/2, 1020089-125. DOI: 10.1504/IJOGCT.2008.016734

3 Mycka, L., Lewandowski, D., Anyszkiewicz, J., Charasińska, J. (2022). Analysis of the Possibilities of Including Recycling of Auto-motive Catalytic Converters in the Cu-Pb-Fe Alloy Converting Process. *World of Metallurgy - ERZMETALL*. 75, 5, 266 - 272.

4 Song, Si J., Nguyen, Viet N. H., Lee, M. S. (2024). Separation of Palladium, Platinum and Rhodium from Metallic Mixture by Selective Dissolution with Hydrochloric Acid Solutions Containing Oxidizing Agents. *Mineral Processing and Extractive Metallurgy Review*, 45, 4, 356 - 367, DOI: 10.1080/08827508.2023.2176852

5 Haile J.M. (1992) *Molecular Dynamics Simulation (Book).* A Wiley-Interscience Publication, New York.

6 Davoodi J., Ahmadi M., Rafii-Tabar H. (2010). Molecular dynamics simulation study of thermodynamic and mechanical properties of the Cu-Pd random alloy. *Materials Science and Engineering: A.* 527(16-17), 4008-4013.

7 Ciftci Y.O., Colakoglu K., Ozgen S., Kazanc, S. (2007). The calculation of some thermoelastic properties and pressure-temperature (P-T) diagrams of Rh and Sr using molecular dynamics simulation. *Journal of Physics: Condensed Matter*. 19(32), 326204, DOI: 10.1088/0953-8984/19/32/326204

8 Cagın T., Dereli G., Uludogan M., Tomak M. (1999). Thermal and mechanical properties of some fcc transition metals. *Physical Review B*. 59, 3468, DOI: https://doi.org/10.1103/PhysRevB.59.3468

9 Daw M.S., Baskes M.I. (1984) Embedded-atom method: Derivation and application to impurities, surfaces, and other defects in metals. *Physical Review B.* 29, 6443. DOI: 10.1103/PHYSREVB.29.6443

10 Finnis M.W., Sinclair J.E. (1984) A Simple Empirical N-Body Potential for Transition Metals. *Philosophical Magazine A.* 50, 45. DOI: http://dx.doi.org/10.1080/01418618408244210

11 Ercolessi F., Parrinello M., Tosatti E. (1988). *Phil. Mag.* A, 58, 213.

12 Sutton A.P., Chen J. (1990). Long-range Finnis-Sinclair potentials. *Philosophical Magazine Letters.* 61(3), 139-146. DOI: https://doi.org/10.1080/09500839008206493

13 Ackland G. J., Finnis M.W. (1986). *Philosophical Magazine A.* 54(2), 301.

14 Rafii-Tabar H., Sutton A.P. (1991). Long-Range FinnisSinclair Potentials for Fcc Metallic Alloys. *Philosophical Magazine Letters.* 63(4), 217-224, DOI: http://dx.doi.org/10.1080/09500839108205994

15 Kob W. (1999). *Journal of Physics: Condensed Matter*, 11(10), R85.

16 Cagın T., Qi Y., Li H., Kimura Y., İkeda H., Johnson W.L., Goddard W.A. (1999). *Jr.,MRS Symp. Ser.* 554, 43.

17 Qi Y., Cagın T., Kimura Y., Goddard III W.A. (1999). Molecular-dynamics simulations of glass formation and crystallization in binary liquid metals: Cu-Ag and Cu-Ni. *Physical Review B.* 59, 3527, DOI: https://doi.org/10.1103/PhysRevB.59.3527

18 Qi, Y., Cagın, T., Kimura, Y., Goddard III W. A. J. (2002). *Comp. Aided Mater.* 8, 233-243

19 Lee H.J., Cagın T., Johnson W.L., Goddard III, W.A. (2003). *J. Chem. Phys.* 119, 9858.

20 Kart H.H., Tomak M., Uludogan M., Cagın T. (2005). *Computational Materials Science*, 32, 107-117.

21 Ozdemir Kart S., Tomak M., Uludogan M., Cagın T. (2006). *Turk J. Phys.* 30, 319-327

22 Davoodi J., Moradi J. (2011). *World Academy of Science, Engineering and Technology.* 54, 354-358.

23 Ning Y., Hu X. (2003). *Platinum Metals Review.* 47, (3), 111-119, DOI: https://doi.org/10.1595/003214003X473122122

24 Luyten J., De Keyzer J., Wollants P., Creemers C. (2009). *Computer Coupling pf Phase Diagrams and Thermochemistry.* 33, 370-376.

25 Sakamoto Y., Ohira K., Kokubu M., Flanagan T.B. (1997). *Journal of Alloys and Compounds.* 253-254, 212-215

26 Andersen H.C. (1980). *J. Chem. Phys.* 72, 2384-2393, DOI: https://doi.org/10.1063/1.439486

27 Parinello M., Rahman A. (1980). Molecular dynamics simulations at constant pressure and/or temperature. *Phys. Rev. Lett.* 45, 1196

28 Nosé S. (1984). A unified formulation of the constant temperature molecular dynamics methods. *J. Chem. Phys.* 81, 511-519, DOI: https://doi.org/10.1063/1.447334

29 Hoover W.G. (1985). Canonical dynamics: Equilibrium phase-space distributions. *Physical Review A.* 31, 1695, DOI: https://doi.org/10.1103/PhysRevA.31.1695

30 Cagın T., Pettitt B.M. (1991). Molecular dynamics with a variable number of molecules. *Molecular Physics.* 72(1), 169-175, DOI: https://doi.org/10.1080/00268979100100111

31 Vines R.F., Wise E.M. (1941). *The Platinum Metals and Their Alloys, The International Nickel Comp.* New York, (CP)

32 Cagın T., Ray J.R. (1988). *Phys. Rev.* A 38, 7940

33 Mehl M.J., Papaconstantopolos D.A. (1996). *Phys. Rev. B* 54, 4519

34 Luo F., Chen X.R., Cai L.C., Wu Q. (2011). *J. At. Mol. Sci.* 2, 10-19

35 Simmons G., Wang H. (1971). *Single Crystal Elastic Constants and Calculated Aggregated Properties, MIT Press*, Cambridge

36 Singh N. (1999). *Pramana J. Phys.* 52, 511

37 Baria J.K., (2004). *Czech. J. Phys.* 54 469-484

38 Chen K., Zhao L.R., Tse J.S., Rodgers J.R. (2004). *Physics Letters A*, 331, 400-403

39 Vitos L., Korzhavyi P.A., Johansson B. (2002). Elastic Property Maps of Austenitic Stainless Steels. *Physical Review Letters*, 88(15), 155501-1, DOI: https://doi.org/10.1103/PHYSREVLETT.88.155501

40 Pettifor D. G.(1992). Theoretical Predictions of Structure and Related Properties of Intermetallics. *Materials Science and Technology*, 8, 345-349, DOI: https://doi.org/10.1179/mst.1992.8.4.345

AUTHORS' INFORMATION

Zhangabay Turar - MSc student, Department of Physics, Sakarya University; ORCID iD: https://orcid.org/0009-0004-6202-112X; (e-mail: zhangabay.turar@ogr.sakarya.edu.tr Phone: +905376890526)

Ali Coruh - Prof.Dr, Department of Physics, Sakarya University, Sakarya, Turkey; SCOPUS Author ID: 24460990900 ORCID iD: https://orcid.org/0000-0002-7362-6173 (e-mail: coruh@sakarya.edu.tr Phone: +9053555943390)
Arystanbek Kussainov - Researcher of Protective and Functional Coatings Scientific Center, D. Serikbayev East Kazakhstan Technical University; Institute of Composite Materials LLP, Ust-Kamenogorsk, Kazakhstan; SCOPUS Author ID: 59515031200. (e-mail: arys20055@gmail.com)
Rakhmetova Mairagul - Dr. Department of Plasma Physics and Computer Physics, Al-Farabi Kazakh National University, Almaty,Kazakhstan/ Department of Physics and Technical disciplines, Kh. Dosmukhamedov Atyrau University, Atyrau, Kazakhstan, ORCID iD: https://orcid.org/0000-0003-4529-0999 (e-mail: maira_12_05@mail.ru)